Arch. Metall. Mater. **70** (2025), 1, 367-374

DOI: https://doi.org/10.24425/amm.2025.152554

R. ARIVUMANI[1,2*], P. ILAMATHI[1], K. BALAMURUGAN[3]

FATIGUE AND FRACTOGRAPHY ANALYSIS OF Al2016-T6 ARTIFICIAL AGE HARDENED AEROSPACE HIGH STRENGTH ALLOY

The primary goal of the research work is, to employ a novel alloy as the skin material of the spaceship as a replacement for Al2024-T3. As a part of this task, a twin rolled Al-Cu wrought alloy, Al2016, was received after being age hardened to T6 condition. This article focuses on the fatigue properties and post-fracture analysis of the Al2016-T6 Alloy. Specimens were prepared according to ASTM E606 standards, and subjected to a rotating-bending fatigue testing machine. As a result, the fatigue property of the Al2016-T6 alloy was determined by Wohler's curve method, fatigue life prediction through the Basquin Equation, estimation of fatigue strength for infinite fatigue life using the Kohout-Věchet model, and fatigue fractography observations via SEM images. The mode of fracture, the origin of fracture and its mechanism, and the morphology of fractured surfaces were reported after investigation. The outcomes of this alloy were compared and discussed with the properties of the existing skin material of the spacecraft, Al2024-T3.

Keywords: Al2016; Age hardening; Basquin equations; Kohout-Věchet fatigue model; Fractography

1. Introduction

After the 1920s, aluminium alloys took the role of wood as the main component of aircrafts. The utilisation of aluminium 2xxx series alloys plays predominant role in aerospace domain from the last six decades. In particular Al-Cu grades of 2618 and 2024 are employed in Concorde aircraft relatively in major scale [1]. At the same time, it has been looked forward a replacement in economic and efficient way. Due to its lower price, smaller weight, and potential for sufficient hardening to increase strength, aluminium is intriguing. It is one of the easily processed and well-performed materials, which typically contributes to lower costs. Fractography and fracture mechanics likely support for knowing the interrelationship of applying cyclic load and surface roughness of specimens [2]. High-strength aluminium alloys will remain significant aerospace materials, even if the use of composite materials is projected to effectively reduce the role of aluminium in emerging aircraft vehicles. The two types of support that modern aircraft manufacturers seek from their suppliers are as follows, to embark on, there are significant cost-cutting initiatives underway for existing aviation models that demand the creation of contemporaneous material selections.

In the aircraft industry, replacing assemblages and architectural structures with integrated or monolithic frameworks is a crucial component of the cost-cutting strategy. A combination of prefabricated sheets and extruded, machined, or connected pieces that are temporarily or permanently linked together make up an assemblage rather usually [3]. Each material has unique qualities that give rise to its own advantages and disadvantages. Choosing the right material for a mechanical system is often a crucial process. Particularly, a detailed overview of the properties of the materials is required for the design and selection of optimum materials for each individual component of a mechanical assembly. By changing their physicochemical properties and processing, materials may often have their features modified to the desired product usage. Furthermore, the demands placed on a part cannot be satisfied by a single material for several applications; rather, a materials process is required, in which multiple components of the solution perform out significant tasks. Characteristics of the alloys can be modified by thermal strengthening and grain refining processes, instead of reinforcing the elements [4]. Age hardening is one of such strengthen treatment for aluminium alloys especially for the combination of Al-Cu, Al-Mg-Si and Al-Zn alloys [5]. The need for

[1] DEPARTMENT OF PRODUCTION ENGINEERING, GOVERNMENT COLLEGE OF TECHNOLOGY, COIMBATORE, 641013, TAMILNADU, INDIA.
[2] DEPARTMENT OF MECHANICAL ENGINEERING, KIT-KALAIGNAR KARUNANIDHI INSTITUTE OF TECHNOLOGY, COIMBATORE, 641402, INDIA
[3] DEPARTMENT OF MECHANICAL ENGINEERING, GOVERNMENT COLLEGE OF ENGINEERING, ERODE, 638316, TAMILNADU, INDIA.

* Corresponding author: sun.arivumani@gmail.com

large-scale transportation services in the twenty-first century must be met concurrently with the need for technical advancements and improved materials [6]. One such cutting-edge, robust material is Al2016 high-strength aluminium alloy, where the elemental constitution and distinct age-hardening processes provide unique characteristics. Al2016 would be a preferable option because it has a superior elemental makeup, especially in terms of Ag and Mg. It is important to process this alloy at different temperatures and times, including artificial and over-aging conditions, in order to investigate the special features of Al2016 [7]. Mechanical characteristics and much higher damage tolerances would be gotten better during T3 to T8 age-hardening conditions.

One of the significant forms of failure is fatigue, which is the degradation or fracture brought on by prolonged cyclic load. A rupture starts to grow and has a tendency to develop if an object is repeatedly loaded cyclically at a specific location of the material. The component eventually fractures at the spot as those cracks progressively enlarge, resulting in failure. Consequently, once engaged in designing a mechanical functioning model, it is crucial to comprehend the fatigue limitations of the alloy. A greater count of cracks would be noticed besides surroundings of the specimen if the value of fatigue life is high; it indicates the multiple crack initiation progress. Hence, deeper dimples in the initiation zone can be identified, those are invisible in the crack growing zone [8]. Engineering alloys may fracture via an intergranular or transgranular fracture pattern. However, in addition to the fracture pattern, additional fracture processes are also implicated in the failure [9]. One type of fracture, called dimple rupture, involves the aggregation and growth of microvoids at the granular interface of the metal. Decohesive rupture, which occurs along weak material surfaces in a reactive environment, is another kind of metal failure. A kind of crystalline failure known as cleavage is associated with brittle fractures which have low energy [9,10]. Each of these modes has a surface failure feature and a unique method for moving forward as the fracture spreads.

Dislocation interactions that include complicated slip and crystallographic connections frequently serve as the foundation for fracture modes. Crack nucleation and crack propagation are typically the two phases of fracture. The start, propagation, coalescence of microvoids, and the micro mechanism of ductile fracture have been proposed; in addition, the relationships across design of voids, condition of stress state and purity of materials have been established [11]. Collective microstructural alterations manifest in the fatigue region as solid strips of slip, realignment of the dislocation set-up within cell formation, nucleation of microvoids, and their extension manifesting as secondary phase inclusions [12,13]. High strain amplitudes, which are often linked to extremely short lifetimes, are related with the latter process. Regardless of the stress amplitude levels, early fracture identification is essential to prevent the structure from breaking. Studies using electron fractography have also provided conclusive experimental testing proof about the beginning processes of fatigue failures. Al2016, an alloy known for its lightweight, has been studied to reveal its desirable characteristics at higher operating temperatures. Relevant microstructure and tensile property information was previously available for these Al2016-T6 and T7 [7]. In this research task this Al2016 material is being experimented with under T6 aging conditions to expose its fatigue capabilities to examine its properties for use as space application skin material.

2. Materials and methods

The elemental proportion of the twin-rolled Al2016 aluminium wrought alloy underwent artificial age hardening at T6 condition is shown in Fig. 1. Fig. 2 illustrated the thermal preparation processes of Al2016-T6 alloy through the Time-Temperature diagram. Initially, an extruded circular bar of Al2016 were solution treated at 505°C for an hour; followed by the alloy at high temperature was quenched to atmospheric temperature. Later, the alloy was exposed to artificial aging by keeping the alloy at 170°C for 24 hours. Hence, the T6 tempered Al2016 alloy was obtained. Consequently, the alloy Al2016-T6 was undergone to stretching process of 1-3% permanent set for stress relieving; and no further straightening was required.

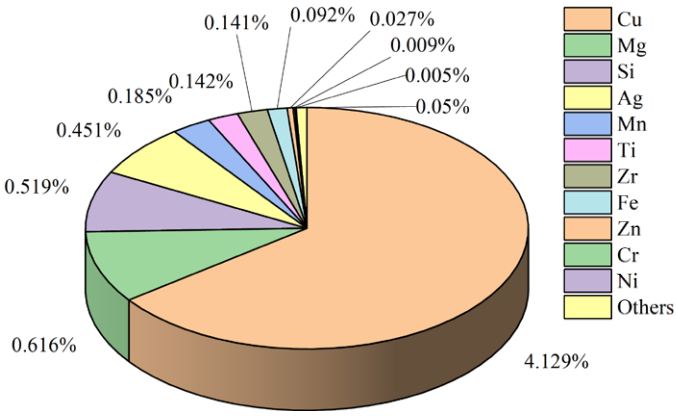

Fig. 1. Elemental composition of Al2016

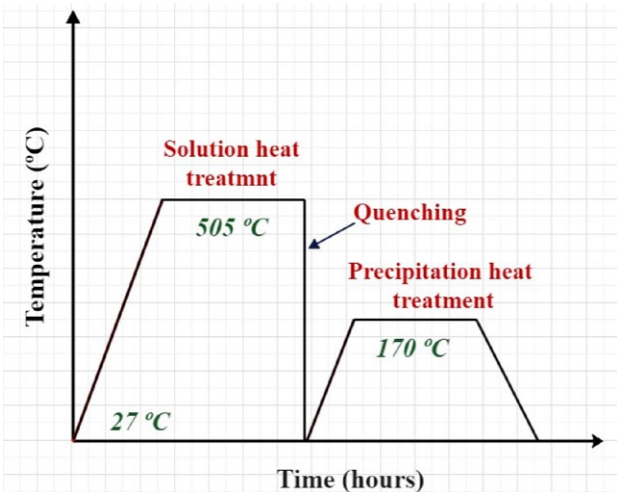

Fig. 2. Time-Temperature diagram of artificial aging process of Al2016 alloy

2.1. Specimen preparation for fatigue testing

80 mm in diameter of a longitudinally grain-oriented cylindrical bar of Al2016-T7 was taken and machined as per the ASTM E606/E606M-12 standard [14]. As illustrated in Fig. 3, nine specimens were precisely machined using an LMW-Smart Turn CNC lathe machine tool and termed as Sp. No (specimen number) E1 to E9, followed by mechanical polishing was done for super finishing. The specimens were hand-ground using silicon carbide sheets while mounted on a bench lathe. 20 to 70 microns of materials were eliminated, resulting in a consistent size with improved finishing [15].

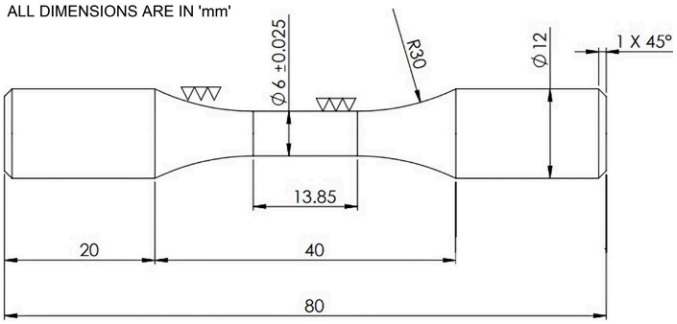

Fig. 3. Fatigue specimen dimension of Al2016-T6 as per ASTM standard E606/E606M-12

A rotating bending fatigue machine with a capacity of 20 Nm was employed at room temperature to find the life of the specimen whether it crosses the cycle of ten million or not. The specimen was properly mounted using the motor spindle ratio and the suitable balancing of the machine's scale. The specimens were subjected to a defined mean load, zero, and alternating loads with the stress ratio of $R = -1$ under constant stress amplitude. The number of cycles required for failure was noted at the end of the testing. The initial working stress amplitude was determined through the tensile property of the alloy. The initial fatigue amplitude was approximately considered around 0.5 times the ultimate tensile strength [7]. The tests were then repeated using similar specimens under various cyclic stresses. The amplitude of the mean and cyclic load will determine whether the specimen's net stress is in the direction of the loading cycle or the opposite. The fatigue tests were conducted until the specimens were either broken or reached ten million cycles, and the result of each specimen was marked to plot the S-N diagram.

In general, fatigue tests were performed to obtain the fatigue limit at ten million cycles. Where the occurrence of failure is limited under these stress amplitudes. Besides, the fatigue limit does not appear until 10^9 cycles for some grades of materials. This phenomenon indicates that the common stress-based equation of fatigue life to stress Eq. (1) is only valid for the middle number of cycles in the S-N curve.

$$\sigma_a = a N_f^b \tag{1}$$

Where σ_a (also referred as σ_f) – Stress amplitude in MPa, N_f – Fatigue life in cycles, a – Fatigue strength coefficient, b – Fatigue strength exponent. Kohout-Věchet developed a common equation (Eq. (2)) to predict the fatigue life of infinite fatigue limit in all the regions of S-N curve (Low Cycle Fatigue, High Cycle Fatigue) [16].

$$\sigma(N) = \sigma_\infty \left[\frac{N + 10^7 \alpha\beta}{N + 10^7 \alpha} \right]^{-b} \tag{2}$$

The values of α and β were derived from Eq. (3) and Eq. (4) respectively.

$$\alpha = \frac{\sigma_c^{-1/b} - \sigma_\infty^{-1/b}}{\sigma_u^{-1/b} - \sigma_c^{-1/b}} \tag{3}$$

$$\beta = \frac{\sigma_u^{-1/b}}{\sigma_\infty^{-1/b}} \tag{4}$$

Where σ_u – ultimate tensile strength, σ_∞ – fatigue limit, σ_c – fatigue strength at 10^7 cycles, $-b$ – slope of the curve; In which σ_c and $-b$ was derived from the least square method.

Since the fatigue strength of the alloy is determined by using the S-N curve method, a stress-based equation is necessary to employ finding the fatigue life. The fatigue life of the alloys was estimated by using the experimental fatigue results. Fatigue life of Al-Cu alloys, derived through the Basquin equation [16]. Though applying this equation is an earlier method, it has been used very often used in calculating fatigue life. In general, during high cycle fatigue, the strain due to plasticity is very small where the illustrated Eq. (1), indicates the connection between the counts of reversal loading ($R = -1$) and alternating stress.

$$b = \frac{h\sum_{i=1}^{h} \log\sigma_{ai} \log N_{fi} - \sum_{i=1}^{h} \log\sigma_{ai} \sum_{i=1}^{h} \log N_{fi}}{h\sum_{i=1}^{h} \left(\log N_{fi}\right)^2 - \left[\sum_{i=1}^{h} \log N_{fi}\right]^2} \tag{5}$$

$$\log a = \frac{\sum_{i=1}^{h} \log\sigma_{ai} - b\sum_{i=1}^{h} \log N_{fi}}{h} \tag{6}$$

The values of the b and a can be derived from the following Eq. (5) and Eq. (6) for h number of specimens used in the testing [17].

2.2. Specimen Preparation for Fatigue Fractography

After being subjected to rotating-bending tests for fatigue, broken specimens were carefully collected. It was cleaned in ultrasonic bath for five minutes. The individual failed specimens were placed into the sample chamber of the Scanning Electron Microscope with one side fastened into the holder. In order to capture the necessary images for further study, micrographs were taken at various positions and magnifications, including 10×, 50×, 100×, 200×, 500×, 1000×, and 2000×.

3. Result and discussion

The fatigue strength of the Al2016-T6 alloy was empirically determined through the S-N curve method (Wohler's curve method) as depicted in Fig. 4. TABLE 1 reported the fatigue test results for each prepared specimen under various load conditions registered. Fig. 4 illustrated the fatigue behaviour of Al2016-T6 alloy along with the S-N curve of Al2024-T3 [18] for delivering the comparison in between. Al2024-T3 natural aging alloy is well known for its fuselage and structural applications, especially as skin materials of space crafts. The fatigue testing method and procedure of Al2024-T3 specimens were as same as Al2016-T6. Fig. 4 reported that the fatigue strength of Al2024-T3 was 138 MPa at room temperature [19].

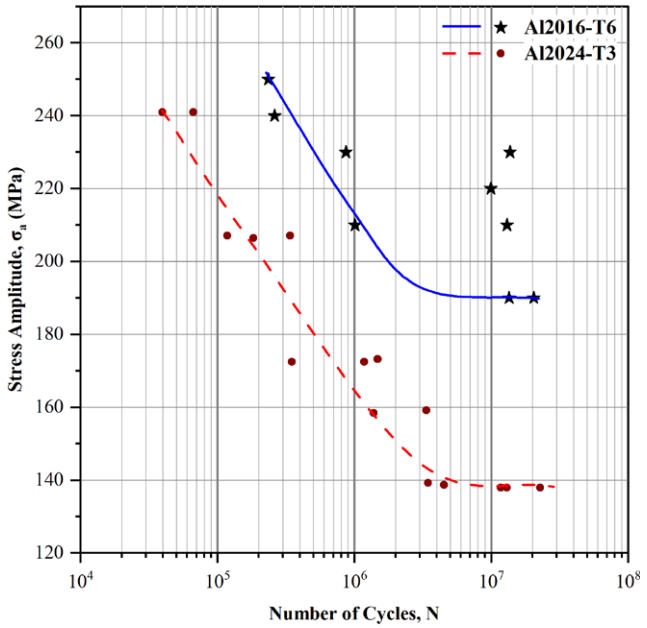

Fig. 4. Fatigue behaviour of Al2016-T6 and Al2024-T3 using Wohler's curve method

TABLE 1 reported the fatigue life in several cycles corresponding to the different stress amplitudes of Al2016-T6 alloy; In which, fatigue strength (σ_f) of Al2016-T6 alloy was obtained by using Wohler's curve and the endurance limit approach. To begin the fatigue experiment, it was considered the initially applied stress amplitude was 48% [20] of its maximum tensile strength; where the ultimate tensile strength of Al2016-T6 was reported as 553.4 ± 3.21 in longitudinal grain orientation [7]. The test is thus commenced with a 250 MPa load. In a gradual decrement, stress amplitudes were applied during the fatigue testing as shown in TABLE 1, which was done until two specimens could run for ten million cycles (1×10^7) without breaking.

The applied stress amplitudes for the Sp. No. E3 and E6 were 230 MPa and 210 MPa respectively; both accomplished ten million cycles. Whereas, at the same exerted reversal loads of 210 MPa and 230 MPa, Sp. No. E4 and E7 had failed to complete the demanded cycles. Only at 190 MPa stress load, both the specimens E8 and E9 consecutively completed the ten million cycles without breaking. Thus, 190MPa was found to be the fatigue strength of Al2016-T6.

Fig. 4 indicated the fatigue behaviour of Al2016-T6 and Al2024-T3 [18] at various stress amplitudes; where the number of cycles corresponding to the stress amplitudes was plotted followed by the S-N curve was generated using a best fitting technique based on Wohler's curve method. At the time of artificial ageing processes Al2016-T6, due to the slight inhomogeneity during the reaction between metallic elements, a few specimens of different stress amplitudes have achieved ten million cycles or the nearby; where three specimens of distinct stresses failed to cross the one million cycles mark two times constantly. Nevertheless, as shown in Fig. 4, a crossing of ten million cycles was made possible for specimens of Al2016-T6 which were corresponding to the stress amplitudes of 190 MPa, 190 MPa, 210 MPa, and 230 MPa.

The Kohout-Věchet fatigue model was proposed in the process of determining the fatigue strength for all the regions, which included low cycle region, high cycle region and finite life cycle region for the infinite fatigue life of the taken alloys. This full-range fatigue life model required the experimental results of fatigue limit and ultimate tensile strength; where the recorded empirical measurement of Al2016-T6 were 190 MPa and 553.4 ± 3.21 MPa respectively.

As shown in Fig. 5 fatigue strength (σ_c) at 10^7 cycles, the slope ($-b$) for the least square line were evaluated using the least square method; as a result, σ_c =234.88 ± 7.77 MPa, and $-b$ = 1.97 ± 0.72 respectively. Hence, the infinite fatigue life for all the regimes of Al2016-T6 was evaluated at the stress amplitude of 213.34 MPa by considering the low and high tensile strength to fatigue limit by using these values in the Eq. (2). As the fatigue strength of Al2016-T6 is decided by using Wohler's curve technique, a stress-based formula is essential for estimating the fatigue life.

Fatigue life of the Al2016-T6 and Al2024-T3 through Basquin equation were depicted in Fig. 6. It reports the outcome of the fatigue life of Al2016-T6 is 108.8 million cycles with respect to the fatigue strength of 190 MPa; where the calculated values of a = 388.203 and b = –0.0386. The estimated fatigue

TABLE 1

Fatigue status of Al2016-T6 at various stress amplitudes

Sp. No.	E1	E2	E3†	E4	E5	E6†	E7	E8†	E9†
σ_a, (MPa)	250	240	230	230	220	210	210	190	190
Number of cycles, N	2.35×10^5	2.61×10^5	1.37×10^7	8.67×10^5	9.93×10^6	1.30×10^7	1.01×10^6	1.35×10^7	2.04×10^7

† Unbroken Specimens

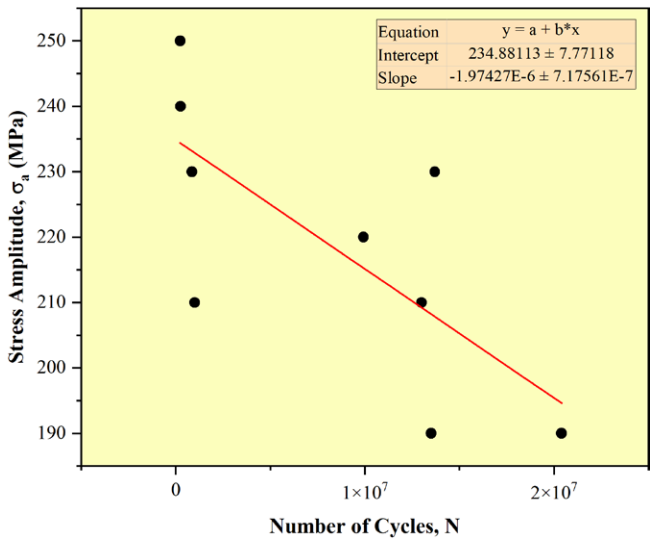

Fig. 5. Least square method to determine the slope and intercept of the Al2016-T6 fatigue test results

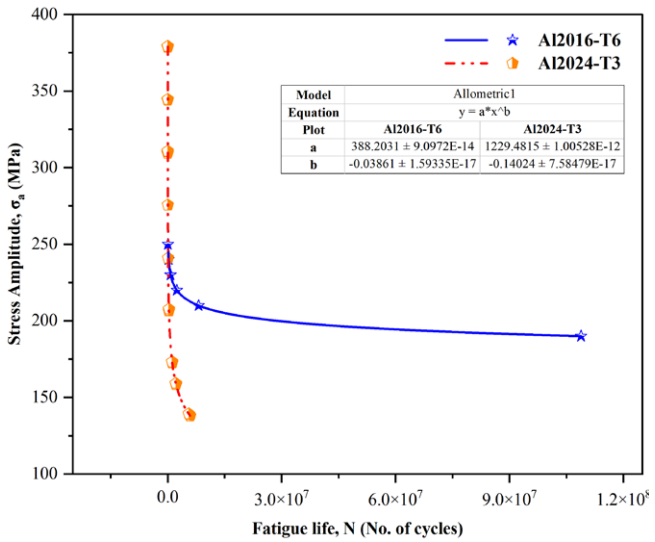

Fig. 6. Fatigue life of Al2016-T6 related with Al2024-T3

life of Al2016-T6 alloy based on the above-derived coefficients is 441 million cycles and 1940 million cycles for 180 MPa and 170 MPa respectively. Obviously, artificial-aged alloys are stronger as well as have more life than naturally-aged alloys.

Fig. 7 moderately revealed the occurrence of intrusions and extrusions which were observed on the zone of fatigue failure-initiated surface. The formation of slip bands was noticed in these patterns. The origination of cracks was taken place from the intrusions. This pattern seems to be a typical feature of how fatigue cracks start. As depicted in Fig. 7(a), distinctive markings known as beach marks and fatigue striations spread outwards from the starting point in a circular arrangement.

In order to locate the points where cracks begin, one can draw an imaginary line perpendicular to their path, originating from the centre. Regardless fractography of Sp. No. E1 indicates the crack initiation zones through Fig. 7. The boundaries between two adjacent failure planes have been marked with a ratchet mark [21]. The ratchet mark can be observed to be located in the middle of the two fracture sources.

Fig. 7(a) more clearly illustrate the same. The occurrence of ratchet markings indicates that several root sources and relatively higher cumulative pressures were involved. The presence of ratchet marks would indicate excessive stress concentrations or extremely high stresses being applied to the component. Notwithstanding, the applied load or the spot of stress concentration determines the main cause of failure.

Up to 0.3% addition of Zr reduces the tiny intermetallic precipitates, which restrict the recovery as well as recrystallization of particles; further, it supports grain structure arrangement [22]. Figs. 8(a) and 8(b) are the broken surface images, which failed at 220 MPa; where the fractures resembled the low-cycle fracture zones. Fig. 8(a) depicted the steplike formation; strong striations where secondary cracks are rarely evident. Fatigue striations were parallel to the edges of the steps. In general, the steplike patterns evolved from a slip mechanism. The steplike formation was noticeable due to its considerable size. Both images indicate the transgranular fracture. The fractured zone displays the format of brittle, striations with a large spacing;

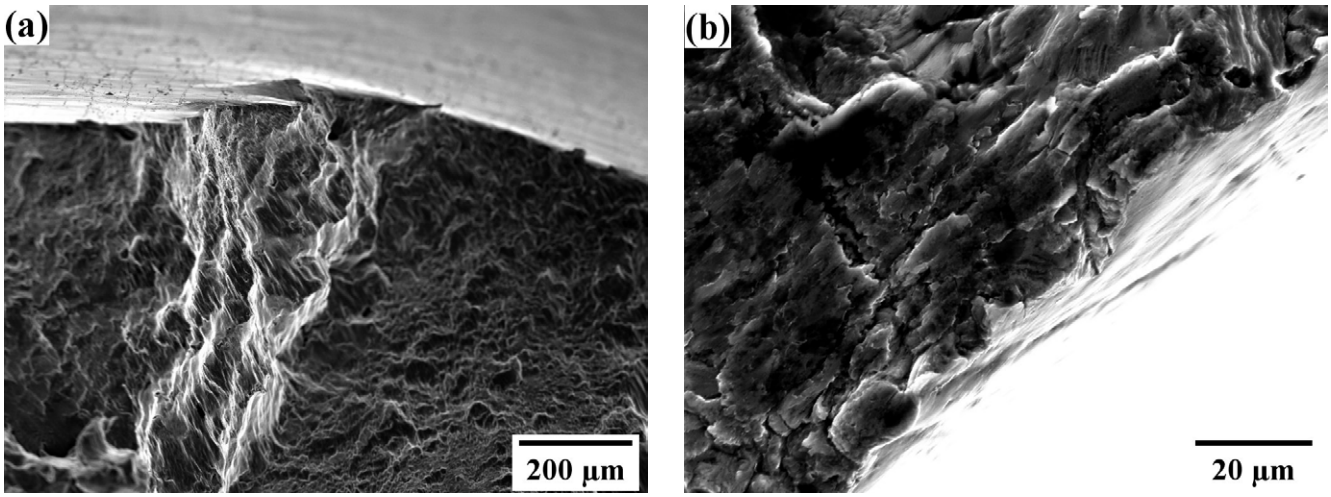

Fig. 7. Al2016-T6 fatigue fractography images of Sp. No. E1 loaded at 250 MPa with the magnifications of (a) 100×, (b) 1000×

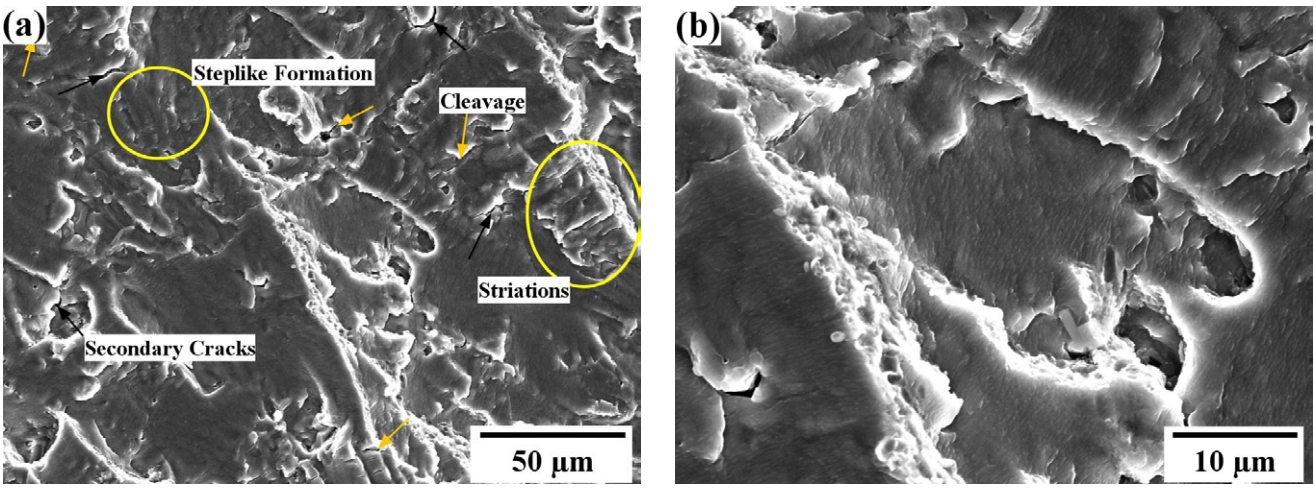

Fig. 8. Al2016-T6 fatigue fractography images of Sp. No. E5 loaded at 220 MPa, with the magnifications of (a) 500×, (b) 1500×

where striations are almost perpendicular to a grain boundary. It is explicit that the cleavage fractures made up each striation. Good amount of Ag facilitates the required attributes of various properties including thermal and chemical [23]. Remarkably, the inclusion of Ag would help to improve mechanical behaviour by altering the microstructure with fine grains. Notably, the presence of spatially structured slabs likely gives rather a superior localization of permanent distortion in the course of alternative stress, because of the deformation of well-ordered precipitates including omega phases in Al-Cu-Mg-Ag alloys [24]; in addition, there will be a emergence of common shear stripes with climb-up stride shapes [25].

Figs. 9(a) and 9(b) exhibited the crack initiation condition where the influence of inclusion caused the crack origin. The

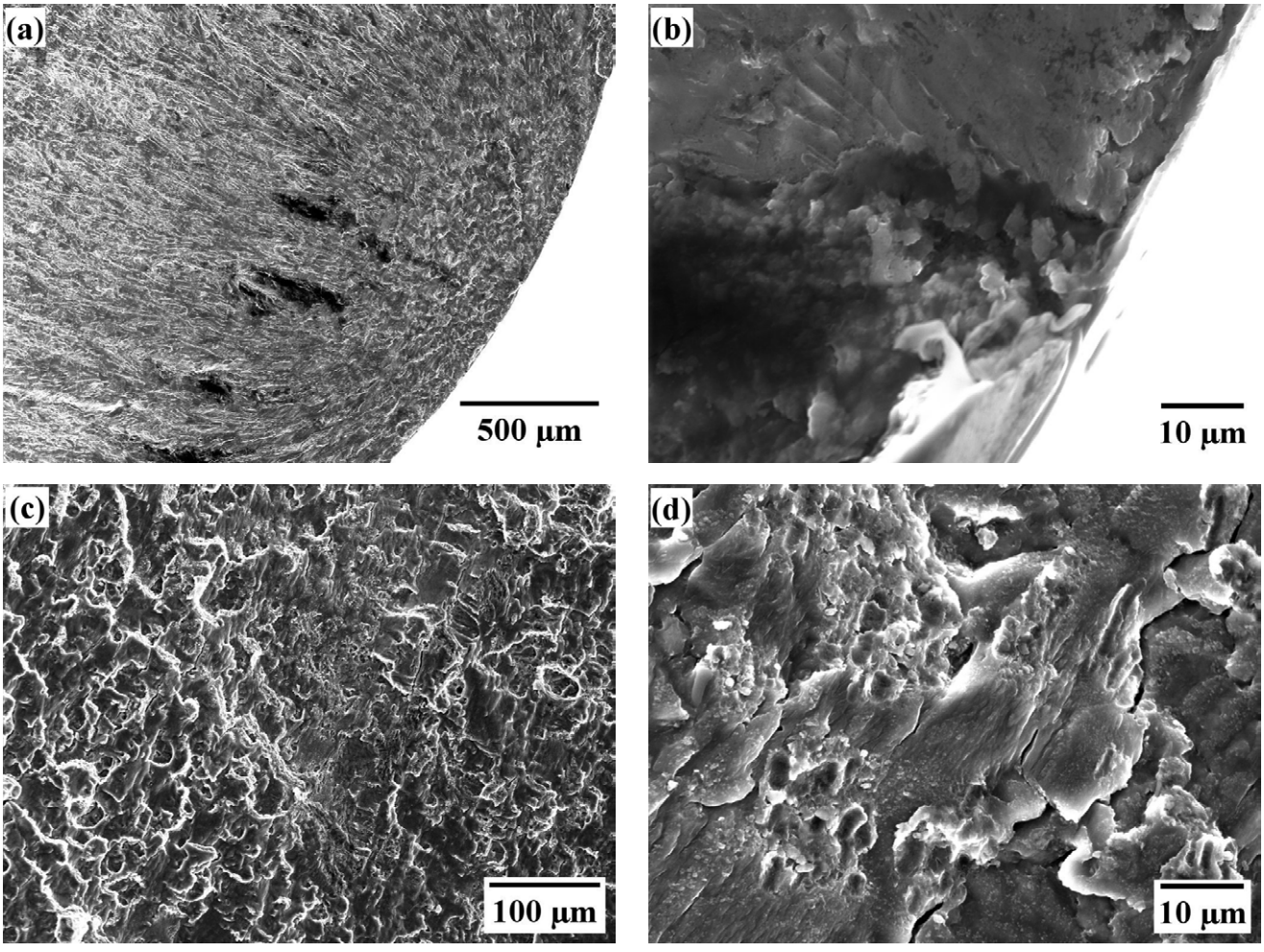

Fig. 9. Al2016-T6 fatigue fractography images of Sp. No. E7 loaded at 210 MPa with magnifications of (a) 50×, (b) 1500×, (c) 200×, (d) 1500×

crack origination, initiation and its mechanisms (such as ratchet marks, fatigue propagation beach marks, and progressive marks) have been discussed above in detail. Figs. 9(c) and 9(d) indicate a portion of the area of final failure at the enlargement of 200× and 1500× respectively. Fractures regions have micro pores and voids that can be dimples of varying dimensions. The vertical face appears to be a significant tear protrusion or cleavage step connecting two dimpled rupture zones. The fracture exhibited ductile properties in nature. Such volatile cracks were promoted owing to nucleated dimples of brittle fractured coarser intermetallic particles. Minute dimples were observed on the distinct regions of the alloy. When observing closely at higher magnifications the fine particles were hardly noticed within the dimples which indicates the ductile intergranular mode of fracture.

Fig. 9(d) exhibited the SEM view of the central area of the fracture surface of Sp. No E7 which crosses the one Million cycles. Despite being a ductile fracture, it exhibits significant secondary cracks that penetrate deeply. The primary pores were initially occupied by alloy second-phase particles, which are now absent. By magnifying the image, it becomes possible to observe the small size of the dimples, typically less than half a micron. It is noteworthy that such a rough fracture surface displays remarkable consistency in the size of these dimples.

Fig. 10 shows intermingled dimples along with ductile striations in high cycle fatigue failures, as well as a high rate of effective load in the crack tip. The alignment of the ductile markings differs in layers. Also, the image reveals that predominantly transgranular dimple rupture to intergranular dimple rupture and crack. In the course of cyclic loading origination of markings such as striations occurred in accordance with the motion of two surfaces concerning each other [26]. These marks were generated by the mechanism of formation which requires the presence of hard inclusions; and a blended style of tension or shears in the direction of crack propagation; or shear force exerted at the right angle to the direction of crack dissemination loading and tension, even though such impressions are caused by a crack extension, likely by fatigue crack development [27]. Al2016-T6 alloy focused on the unique characteristics of ductile failure in the region of unstable crack propagation, which was caused by the formation of dimples predominantly from the coarser intermetallic particles that fractured in a brittle manner. Smaller dimples, resting on defined planes, were seldom observed inside the region. These can be connected to the current tiny particles that, in a few instances, were seen inside the dimples in high magnification photos and imply ductile intergranular fracture.

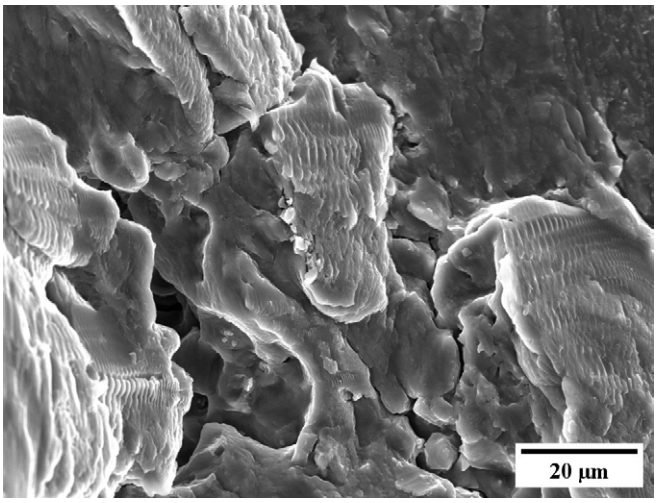

Fig. 10. Al2016-T6 fatigue fractography image of Sp. No. E2 loaded at 240 MPa 2000× magnifications

Upon careful inspection, it becomes apparent that both intrusions and extrusions are present, and fatigue cracks originate from the intrusions and extend into the slip band. This pattern seems to be a common trait in the initiation of fatigue cracks. In fact, research has shown that the fatigue life of a material can be significantly enhanced by periodically removing a small portion of the metal surface. However, implementing such a practice commercially is challenging [28,29]. The size and shape of the striations will differ concerning surrounding and alloy composition. Depending on the kind of alloy and the surrounding environment, striations might have different visual characteristics. The microstructure of Al2016-T6 specimens appeared as slightly limited equiaxed, sphere-shaped grains and bear a resemblance to a griddle-shaped grain structure [7]. The occurrence of intrusions and extrusions was observed on the fatigue failure surface. The formation of slip bands was noticed in these patterns. The origination of cracks was taken place from the intrusions. This pattern seems to be a typical feature of how fatigue cracks start.

4. Conclusion

In the process of investigating the fatigue behaviour of the Al2016-T6 alloy, a stress-based approach was applied. In which, Wohler's curve method was applied to find the fatigue strength empirically. The Kohout-Věchet fatigue method was applied for evaluating the exact fatigue strength of the alloy at infinite fatigue life by considering all the regions. Whilst, Basquin equation was executed in the determination of the projection of fatigue life by taking into account the middle portion of the S-N curve. The results from each method were related with Al2024-T3. 190 MPa was derived as the fatigue strength through Wohler's curve method. According to Kohout-Věchet model, fatigue strength for infinite life in all the regions (including LCF and HCF) of the S-N curve were estimated as 213.34 MPa. By applying Basquin equation, fatigue life of Al2016-T6 was derived corresponding to the fatigue strength as 108.8 million cycles for 190 MPa.

In general inclusions caused the crack origins. Due to high local stress concentration, specimens were broken quickly at 10^5 series cycles. Both become the reasons for the generation of ratchet patterns. At crack propagation regions that smooth and slower fatigue fracture propagation due to the process of artificial aging. Concentric rings are visible in this alloy due to the ductile nature; Beach patterns and fatigue striations extend outward from source point in the form of concentric arcs. Dimple striations, dimples voids, and ductile fractures were prevalently

noticed on the broken specimens, especially which exceeded one Million cycles. Zr involves in recovery and recrystallization and supports grain structure arrangement. Presence of Ag would serve in reshaping the microstructure with fine particles, which results in the betterment of mechanical attributes. The broken alloys exhibited ductile properties with intergranular mode of fracture. In addition, Transgranular fracture and cleavage fractures were noticed. Predominantly, transgranular dimple rupture to intergranular dimple rupture and crack were reported; where micropores and voids at fractures regions were found.

REFERENCES

[1] B. Malek, C. Mabru, M. Chaussumier, Fatigue behavior of 2618-T851 aluminum alloy under uniaxial and multiaxial loadings. Int. J. Fatigue **131**, 105322 (2020). DOI: https://doi.org/10.1016/j.ijfatigue.2019.105322

[2] W. Macek, Fracture surface formation of notched 2017A-T4 aluminium alloy under bending fatigue. Int. J. Fracture. **234** (1-2), 141-157 (2022). DOI: https://doi.org/10.1007/s10704-021-00579-y

[3] Zhou, Wenbin, et al, Advances and trends in forming curved extrusion profiles. Materials **14**(7) 1603 (2021). DOI: https://doi.org/10.3390/ma14071603

[4] Zhou, Wenbin, et al., Manufacturing a curved profile with fine grains and high strength by differential velocity sideways extrusion. Int. J. Mach. Tool. Manu. **140**, 77-88 (2019). DOI: https://doi.org/10.1016/j.ijmachtools.2019.03.002

[5] N.S. Kumar, et al., A critical review on heat treatment of aluminium alloys. Mater. Today-Proc. (2022). DOI: https://doi.org/10.1016/j.matpr.2021.12.586

[6] W. Miller, et al., Recent development in aluminium alloys for the automotive industry. Mat. Sci. Eng. A. **280** (1), 37-49 (2000). DOI: https://doi.org/10.1016/S0921-5093(99)00653-X

[7] A. Ravanan, I. Palanivel, B. Kulendran, Microstructure, Tensile, and Fractography Analysis of Al2016 and Al2618 Age Hardened Aluminium Alloys. Chiang. Mai. J. Sci. **49** (4), 1217-1232 (2022). DOI: https://doi.org/10.12982/CMJS.2022.066

[8] W. Macek, et al., Fracture surface topography investigation and fatigue life assessment of notched austenitic steel specimens. Eng. Fail. Anal. **135**, 106121 (2022). DOI: https://doi.org/10.1016/j.engfailanal.2022.106121

[9] R. Wanhill, Fatigue and fracture properties of aerospace aluminium alloys. NLR Technical Publication TP 93356 L (1993).

[10] K. Lee, H. Takahashi, Fracture and strength'90. Proceedings (1991).

[11] H. Takahashi, K.Y. Lee, Fracture and Strength'90. Fracture and strength'90 (1991).

[12] M. Klesnil, P. Lukác, Fatigue of metallic materials. Elsevier **104** (4), 680-681 (1992). DOI: https://doi.org/10.1115/1.3256408

[13] J. Polak, Cyclic plasticity and low cycle fatigue life of metals. Elsevier Amsterdam 1991.

[14] ASTM, A., E606/E606M–12: Standard Test Method for Strain-Controlled Fatigue Testing. ASTM international, West Conshohocken (PA USA): Book of Standards. 3 (2012). DOI: https://doi.org/10.1520/E0606_E0606M-21

[15] ASTM, E., Standard guide for electrolytic polishing of metallographic specimens. (2009). DOI: https://doi.org/10.1520/E1558-09R21

[16] W. Cui, A state-of-the-art review on fatigue life prediction methods for metal structures. J. Mar. Sci. Technol. **7**, 43-56 (2002). DOI: https://doi.org/10.1007/s007730200012

[17] S. Kwofie, H. Chandler, Fatigue life prediction under conditions where cyclic creep–fatigue interaction occurs. Int. J. Fatigue **29** (12), 2117-2124 (2007). DOI: https://doi.org/10.1016/j.ijfatigue.2007.01.022

[18] S. Kłysz, Transformation of the SN curves for AL 2024 alloy. J. Konbin. **32** (1), 19-36 (2014).

[19] DOT/FAA/AR-MMPDS-01, Metallic Materials Properties Development and Standardization (MMPDS). Federal Aviation Administration Washington, DC. 2003.

[20] G.M.D. Almaraz, V.H.M. Lemus, J.J.V. Lopez, Rotating bending fatigue tests for aluminum alloy 6061-T6, close to elastic limit and with artificial pitting holes. Procedia. Engineer. **2** (1), 805-813 (2010). DOI: https://doi.org/10.1016/j.proeng.2010.03.087

[21] B. Moreno, J. Zapatero, J. Dominguez, An experimental analysis of fatigue crack growth under random loading. Int. J. Fatigue **25** (7), 597-608 (2003). DOI: https://doi.org/10.1016/S0142-1123(03)00018-5

[22] H. Zhang, et al., Effect of Zirconium addition on crack, microstructure and mechanical behavior of selective laser melted Al-Cu-Mg alloy. Scripta. Mater. **134**, 6-10 (2017). DOI: https://doi.org/10.1016/j.scriptamat.2017.02.036

[23] R. Ferragut, et al. Mechanisms of age-hardening in two Al-Cu-Mg alloys studied by Positron Annihilation Spectroscopy. In Mater. Sci. Forum. 2002. Transtec Publications (1999). DOI: https://doi.org/10.4028/www.scientific.net/MSF.396-402.777

[24] M. Gazizov, R. Kaibyshev, The precipitation behavior of an Al–Cu–Mg–Ag alloy under ECAP. Mat. Sci. Eng. A. **588**, 65-75 (2013). DOI: https://doi.org/10.1016/j.msea.2013.09.021

[25] J. Polák, J. Man, Mechanisms of extrusion and intrusion formation in fatigued crystalline materials. Mat. Sci. Eng. A. **596**, 15-24 (2014). DOI: https://doi.org/10.1016/j.msea.2013.12.005

[26] S. Stoyan, D. Kujawski, J. Mallory, Fatigue Crack Growth in 2324 Aluminum Alloy, Western Michigan University. Technical Report No. MAE-05-01 (2005).

[27] A. Shyam, et al., Small fatigue crack growth in metallic materials: A model and its application to engineering alloys. Acta. Mater. **55** (19), 6606-6616 (2007). DOI: https://doi.org/10.1016/j.actamat.2007.08.022

[28] M. Moeser, Fractography with the SEM (failure analysis). Mater. Sci.Monog. 40 (2007).

[29] Handbook, A., volume **12**: Fractography. ASM International. 517, 654 (1987).